Details of the Collagen and Elastin Architecture in the Human Limbal Conjunctiva, Tenon's Capsule and Sclera Revealed by Two-Photon Excited Fluorescence Microscopy

Choul Yong Park,[1] Catherine M. Marando,[2] Jason A. Liao,[2] Jimmy K. Lee,[2] Jiwon Kwon,[3] and Roy S. Chuck[2]

[1]Department of Ophthalmology, Dongguk University, Ilsan Hospital, Goyang, Gyunggido, South Korea
[2]Department of Ophthalmology and Visual Sciences, Montefiore Medical Center, Albert Einstein College of Medicine, Bronx, New York, United States
[3]Department of Ophthalmology, Seonam University, Myongji Hospital, Goyang, Gyunggido, South Korea

Correspondence: Roy S. Chuck, Department of Ophthalmology and Visual Sciences, Montefiore Medical Center, Albert Einstein College of Medicine, Bronx, NY 10467, USA; rchuck@montefiore.org.

Submitted: April 7, 2016
Accepted: August 9, 2016

Citation: Park CY, Marando CM, Liao JA, Lee JK, Kwon J, Chuck RS. Details of the collagen and elastin architecture in the human limbal conjunctiva, Tenon's capsule and sclera revealed by two-photon excited fluorescence microscopy. *Invest Ophthalmol Vis Sci*. 2016;57:5602–5610. DOI:10.1167/iovs.16-19706

Purpose. To investigate the architecture and distribution of collagen and elastin in human limbal conjunctiva, Tenon's capsule, and sclera.

Methods. The limbal conjunctiva, Tenon's capsule, and sclera of human donor corneal buttons were imaged with an inverted two-photon excited fluorescence microscope. No fixation process was necessary. The laser (Ti:sapphire) was tuned at 850 nm for two-photon excitation. Backscatter signals of second harmonic generation (SHG) and autofluorescence (AF) were collected through a 425/30-nm and a 525/45-nm emission filter, respectively. Multiple, consecutive, and overlapping (*z*-stack) images were acquired. Collagen signals were collected with SHG, whereas elastin signals were collected with AF.

Results. The size and density of collagen bundles varied widely depending on depth: increasing from conjunctiva to sclera. In superficial image planes, collagen bundles were <10 μm in width, in a loose, disorganized arrangement. In deeper image planes (episclera and superficial sclera), collagen bundles were thicker (near 100 μm in width) and densely packed. Comparatively, elastin fibers were thinner and sparse. The orientation of elastin fibers was independent of collagen fibers in superficial layers; but in deep sclera, elastin fibers wove through collagen interbundle gaps. At the limbus, both collagen and elastin fibers were relatively compact and were distributed perpendicular to the limbal annulus.

Conclusions. Two-photon excited fluorescence microscopy has enabled us to understand in greater detail the collagen and elastin architecture of the human limbal conjunctiva, Tenon's capsule, and sclera.

Keywords: collagen, conjunctiva, elastin, sclera, Tenon

The conjunctiva, Tenon's capsule, and sclera make up the outermost structures of the human eye. These three layers provide defense against trauma and microorganism invasion, as well as lubrication and blood supply.[1,2]

Collagen and elastin are two major components of the conjunctiva, Tenon's capsule, and sclera.[3,4] These two fibrous proteins are principal contributors to the biomechanical properties of this tissue, especially collagen fibers in the form of collagen bundles (5–35 μm thick), which are grouped into layers of collagen lamellae.[5] Previous methods of studying collagen and elastin fibers in these tissues have been histologic examination (with special staining); immunohistochemistry; or electron microscopy.[4] These conventional approaches afford sagittal images of the conjunctiva, Tenon's capsule, and sclera, which have contributed greatly toward our understanding of the pathogenesis of myopia, pterygium, and chronic open angle glaucoma.[6–9]

However, little is known about the tangential architecture of collagen and elastin fibers of the conjunctiva, Tenon's capsule, and sclera, despite the fact that the tangential plane is what the surgeon views under the operating microscope. The lack of an adequate imaging modality is the primary reason for our poor understanding of the tangential architecture. In addition, the tissue fixation process and the subsequent dehydration of these delicate layers distort the natural collagen and elastin distribution patterns, further limiting our understanding of the natural architecture.

Recently, two-photon excitation fluorescence microscopy (TPEM) has been used to image tangential planes of the cornea and trabecular meshwork.[10,11] Two-photon excitation fluorescence microscopy utilizes near infrared laser (Ti:sapphire) with ultrashort pulse duration (femtosecond) allowing for high-resolution images equivalent to confocal microscopy with wider depth of focus and minimal tissue damage.[12] The tissue of interest can be imaged on a flat-mount without additional tissue processing, hence preserving the three-dimensional (3D) tissue relationships found in vivo. By serial *z*-axis scanning of tangential images and subsequent 3D reconstructions, TPEM provides new insight into ocular microanatomy including fiber orientation. Autofluorescence (AF) imaged by TPEM effectively detects elastin fibers and second harmonic generation (SHG) imaging best portrays collagen structures.[10–14]

Table 1. Clinical Characteristics of Donor Corneal Tissue Used in Study

Sample No.	Age	Race	Sex	Laterality	Harvest to Imaging Time, d	Past Medical History
1	60	White	F	OD	4	Asthma, glaucoma
2	55	White	F	OS	5	Hypertension seizure
3	59	White	M	OD	10	DM, hypertension, anxiety
4	64	White	F	OS	8	Hypertension, GERD, DM
5	39	White	M	OD	5	Chronic back pain
6	73	White	F	OD	4	Head and neck cancer, hypothyroidism, hyperlipidemia
7	67	Black	M	OS	4	CHF, hypertension, DM, hypothyroidism, ESRD

CHF, congestive heart failure; DM, diabetes mellitus; ESRD, end stage renal disease; GERD, gastroesophageal reflux disease.

In this study, we evaluated the conjunctiva, Tenon's capsule, and sclera by using TPEM in human ex vivo cadaveric eyes. The obtained images elucidate new details of the collagen and elastin architecture of these tissues.

Materials and Methods

This study was approved by the institutional review board of Albert Einstein College of Medicine, Yeshiva University, and adhered to the tenets of Declaration of Helsinki.

Sample Preparation

Five eye bank corneal buttons and two eye bank corneal buttons (Table 1) were obtained from the Lions Eye Bank (Tampa, FL, USA) and Saving Sight, (Kansas City, MO, USA) respectively. All tissue samples were kept in a storage chamber with transfer media (Optisol GS; Bausch & Lomb, Rochester, NY, USA) until imaging. All imaging was completed within 10 days of harvesting corneal tissue.

Two-Photon Excitation Fluorescence Microscope Imaging

Imaging of SHG and AF were performed using an inverted two-photon excitation fluorescence microscope (FluoView FV-1000; Olympus, Central Valley, PA, USA). The detailed imaging procedure has been previously reported.[15–17] Briefly, tissue samples were placed on glass-bottom plates (35 mm; MatTek, Ashland, MA, USA) with the imaging area faced down. The laser (Ti:sapphire) was tuned to 850 nm and emission was passed through a red (RDM, 690 nm) filter. A ×25 (numerical aperture = 1.05) water immersion objective was used to focus the excitation beam and to collect backward signals. The backward SHG signal was directed to a dichroic mirror (dm)458 and second harmonic light was collected using a 410- to 440-nm bandpass filter. The backward AF signal was directed to a dm560 and AF was collected using a 503- to 547-nm bandpass filter. Multiple, consecutive, and overlapping tangential image stacks (*z*-stack) were acquired using the same objective lens (Fig. 1). When *z*-stacked images were acquired, samples were scanned in 1- to 5-μm step sizes in the *z*-axis to generate 3D data sets. ImageJ software (http://imagej.nih.gov/ij/; provided in the public domain by the National Institutes of Health, Bethesda, MD, USA) was used to analyze the acquired images.

Image Analysis

The planes from subconjunctiva to superficial sclera were divided into four depth groups. Because the thickness of the conjunctiva, Tenon's capsule, and sclera varied depending on imaging area and samples, depths 1, 2, 3, and 4 were respectively defined as approximately 5%, 35%, 75%, and 95%

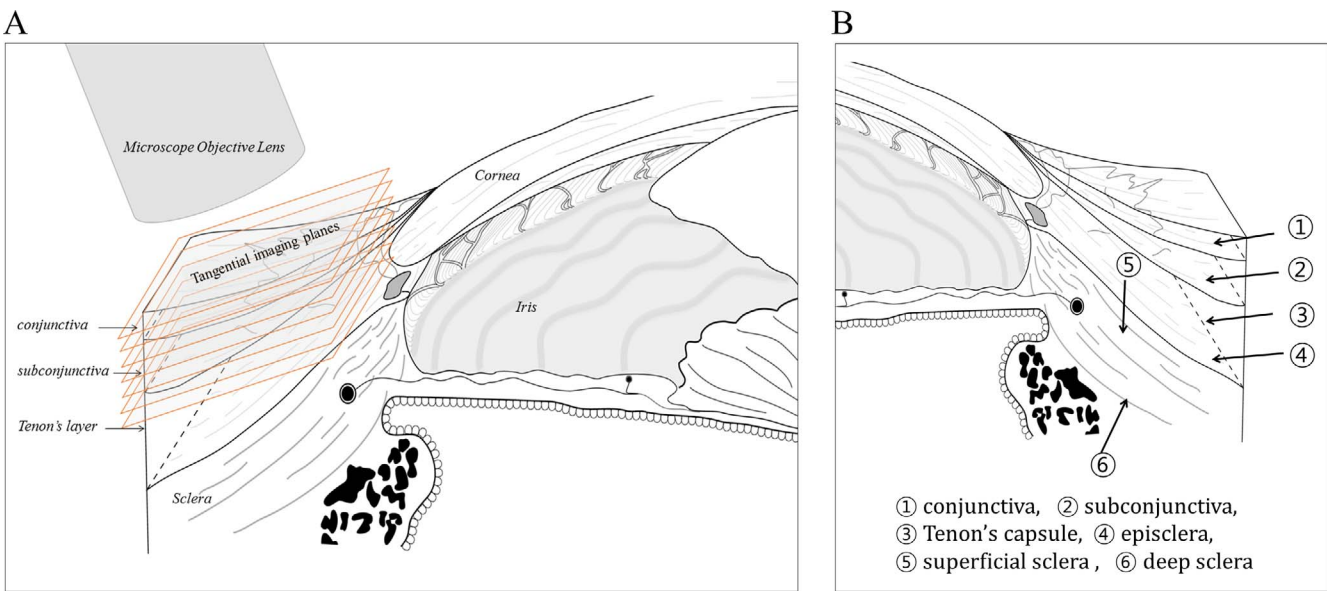

Figure 1. (**A**) Schematic picture of anterior segment structures around the limbus and tangential imaging planes (*red*). (**B**) The locations of images taken in this study.

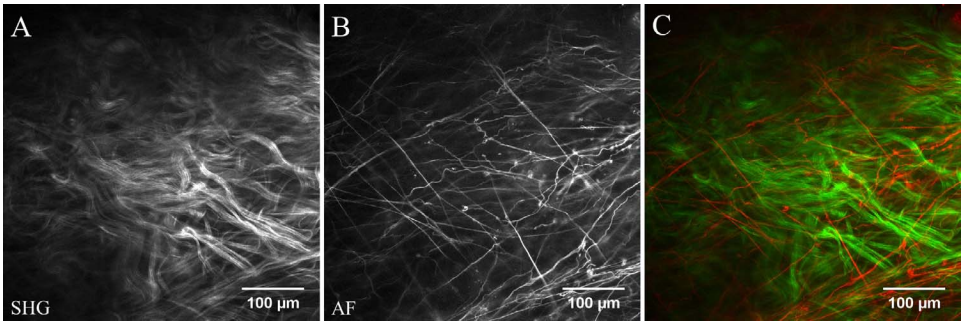

FIGURE 2. Two-photon excitation fluorescence microscopic image of episclera. (**A**) Second harmonic generation image showing thick wavy collagen bundles with high signal intensity. Elastin fibers are invisible in these SHG images. (**B**) Autofluorescence image shows the elastin fiber network with high signal intensity. Relatively medium to low signal collagen bundles are visible in the background. (**C**) Merged image of (**A**) shown in *green* and (**B**) shown in *red*. Collagen and elastin structures are readily distinguished with independent orientations. Images were taken from sample 1 at 120 μm below the conjunctival epithelium.

depth from the en face plane of the first SHG images visible under conjunctiva. Depths 1, 2, 3, and 4 approximately represent conjunctiva, Tenon's capsule, episclera, and superficial sclera, respectively. The diameters of 10 randomly selected collagen fibers per SHG image were calculated using ImageJ software. Images from all seven donors were analyzed and the mean values were compared between each depth. In addition, the SHG images were processed for further analysis using ImageJ software. To simplify indirect estimation of collagen fiber density and arrangement, we adopted the following pattern analysis. Briefly, grayscale SHG images were processed by sequential application of image modifications. First, an image was processed by application of spatial frequency filters (ImageJ → Process → Fourier transform → Bandpass filter). ImageJ bandpass filters have the capacity to remove both high and low spatial frequencies. The filter sets for large and small structures were set at 40 and 7 pixels, respectively. Suppression stripes were set to "none" and tolerance of direction was set at 5%. "Autoscale after filtering" and "saturate image when autoscaling" were activated during processing. Second, the filtered images were converted to binary (ImageJ → Process → Binary → Make binary). Next, a particle count was performed (ImageJ → Analyze → Analyze particle). The set for size was 0 to infinity and the set for circularity was 0 to 1. The counted particle represented the collagen fiber count of the image. Thin and loose collagen fibers in the superficial layers resulted in more individual fibers and larger particle count, whereas thick and compact collagen fibers in the deep layers resulted in less individual fiber numbers and a smaller particle count. In addition, coherency (%) and orientation (degrees) of collagen fibers were also calculated (ImageJ → Plugin → OrientationJ → OrientationJ dominant direction).

Statistical Analysis

Statistical analysis was performed using statistical software (SPSS version 20.0; SPSS, Inc., Chicago, IL, USA). An assessment of normality of data was performed using the Shapiro-Wilk test. Since fiber thickness and pattern analysis data do not show normal distribution, ranked data were used for the comparison of means performed by 1-way ANOVA test with Bonferroni correction. Values of $P < 0.05$ were considered significant.

RESULTS

Images of SHG and AF revealed collagen and elastin fibers and their orientations in conjunctiva and Tenon's capsule. Collagen fibers showed relatively high intensity in SHG and moderate intensity in AF, while elastin fibers showed relatively high intensity in AF and relatively low intensity in SHG images (Fig. 2). The nontransparent sclera hindered the fine image acquisition of middle and deep sclera; however, the SHG technique could obtain images with recognizable collagen bundles down to and a bit beyond 100-μm depth of superficial sclera.

Collagen and Elastin Architecture of Conjunctiva and Tenon's Capsule

The tangential *z*-stack of images revealed the detailed architecture of collagen fibers and bundles (Fig. 3). The size and density of collagen bundles increased from conjunctiva to sclera. In the superficial layers (conjunctiva and Tenon's capsule), the width of most collagen bundles were measured to be less than 10 μm, and were arranged in a loose, wavy, and disorganized pattern. In the deeper layers (episclera and sclera), collagen bundles were found to be thicker and more organized (some bundles 100 μm in width) and were more densely packed (Fig. 3; Table 2, Supplementary Videos S1, S2) The average orientation and coherence of collagen fibers were not statistically significant at different imaged depths (Table 2). The change in collagen fiber appearance was prominent in the 3D analysis (Fig. 4). The thin and wavy collagen fibers at the superficial conjunctiva and Tenon's layer were gradually replaced by thicker and straighter scleral collagen fibers.

Compared with the collagen architecture, individual elastin fibers were thinner and straighter and the distribution looser and more sparse (Fig. 5). Interestingly, the pattern of the elastin fiber network was independent of that of the collagen fiber network in the superficial layers, such as Tenon and superficial sclera (Fig. 5). However, elastin fibers near the limbal area were compact and oriented perpendicular to the limbus (Fig. 6). Collagen fibers at the limbus were also oriented perpendicular to the limbus, albeit more sinusoidal and dense.

Collagen and Elastin Architecture of Sclera

Collagen bundles in the superficial sclera showed a densely packed sinusoidal arrangement (Figs. 7A, 7C). The elastin fibers in this layer were elongated and crossed collagen bundles at an almost perpendicular angle (Figs. 7B, 7C). In the deeper sclera, collagen bundles lost their sinusoidal pattern and were instead arranged in a "woven basket" appearance with thicker and linear fiber distribution (Figs. 7D, 7F). In the deeper sclera, collagen bundles contained relatively small

Investigative Ophthalmology & Visual Science

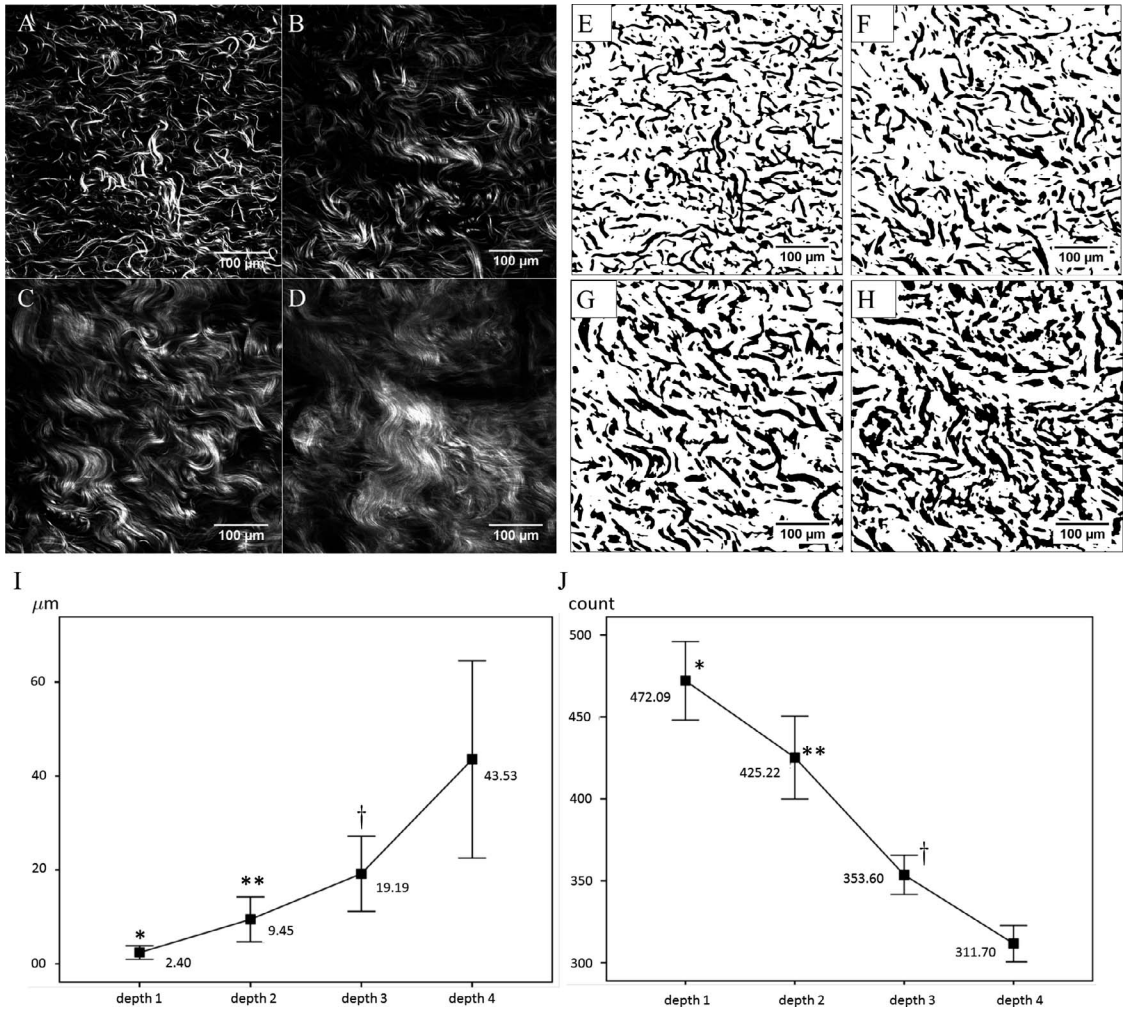

Figure 3. Second harmonic generation images of conjunctiva, Tenon's capsule, episclera, and sclera. (**A**) Conjunctiva (10 μm below epithelium). (**B**) Tenon's capsule (60 μm below epithelium). (**C**) Episclera (120 μm below epithelium). (**D**) Sclera (180 μm below epithelium). Collagen bundles are thin and loose at superficial layers (**A**, **B**), but become thick and compact at deeper layers (**C**, **D**). Collagen bundles in superficial sclera appeared to have a medium-frequency sinusoidal pattern, whereas deeper sclera had a lower-frequency sinusoidal pattern (**C**). (**E**–**H**) Images from (**A**–**D**) were transformed for pattern analysis. (**I**) Collagen fiber diameters increased from depth 1 to 4. (**J**) Pattern analysis shows significant decrease of fiber count from depth 1 to 4. Images were taken from sample 2. Analysis was performed using seven donor corneas (**I**, **J**). *Black square*: mean value. *Error bars*: standard deviation. * $P < 0.001$ versus depths 2, 3, and 4. ** $P < 0.001$ versus depths 3 and 4. † $P < 0.001$ versus depth 4.

Table 2. Collagen Fiber Pattern and Thickness at Different Image Planes From Conjunctiva to Superficial Sclera

	Depth 1	Depth 2	Depth 3	Depth 4	*P* Values*
Fiber count, No.					
Mean ± SD	480.17 ± 43.38	425.17 ± 22.42	331.67 ± 52.61	292.33 ± 51.02	<0.001
Range	418–590	402–476	210–372	145–328	
Fiber orientation, deg					
Mean ± SD	−15.59 ± 26.79	−21.03 ± 24.86	−17.91 ± 14.85	−22.23 ± 29.84	0.923
Range	−40.05 to 29.06	−41.51 to 20.89	−36.40 to −5.68	−43.62 to 22.98	
Fiber coherency, %					
Mean ± SD	0.15 ± 0.03	0.13 ± 0.04	0.19 ± 0.03	0.17 ± 0.06	0.348
Range	0.10–0.20	0.06–0.18	0.16–0.23	0.10–0.28	
Fiber thickness, μm					
Mean ± SD	2.24 ± 1.36	8.97 ± 4.50	18.65 ± 7.40	46.46 ± 20.64	<0.001
Range	0.56–5.56	3.57–23.57	9.07–36.79	15.72–98.57	

Depths 1, 2, 3, and 4 were defined as 5%, 35%, 75%, and 95% depth from the en face plane of the first SHG images visible under the conjunctiva, representing conjunctiva, Tenon's capsule, episclera, and superficial sclera, respectively.

* *P* values were calculated by using the Kruskal-Wallis test.

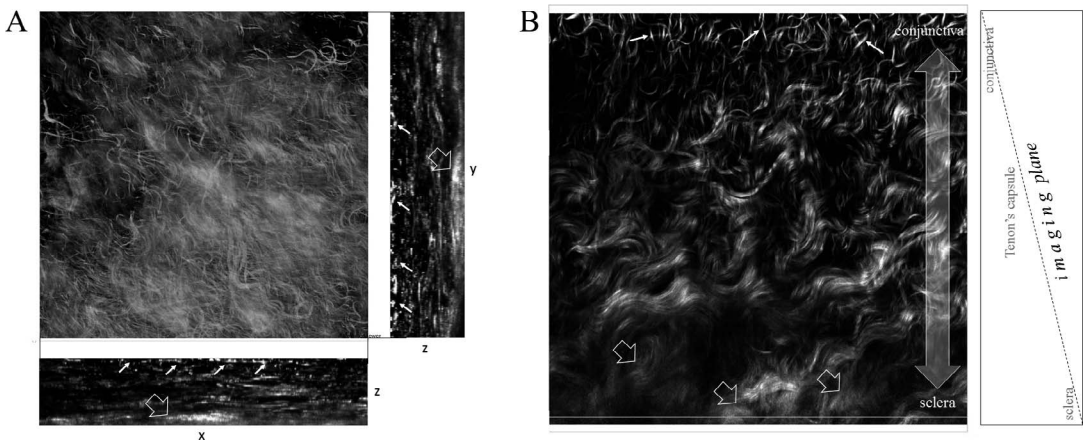

Figure 4. Three-dimensional reconstruction of SHG images from Tenon's layer to superficial sclera. (**A**) Three-dimensional reconstructed image with cross-sectional images of the right side (*y-z* plane) and the bottom side (*x-z* plane). Thin collagen fibers at Tenon's layer (*white arrows*) are contrasted with thick collagen fibers of superficial sclera (*blank arrow*). (**B**) En face shot of the 3D reconstructed image with a slanted image plane, starting with the conjunctiva (*upper border*) and ending with the superficial sclera (*lower border*). This frame reveals the thin collagen fibers in conjunctiva and Tenon's layer (*white arrows*) that gradually change to thick superficial scleral collagen fibers (*blank arrows*). Images were taken from sample 2.

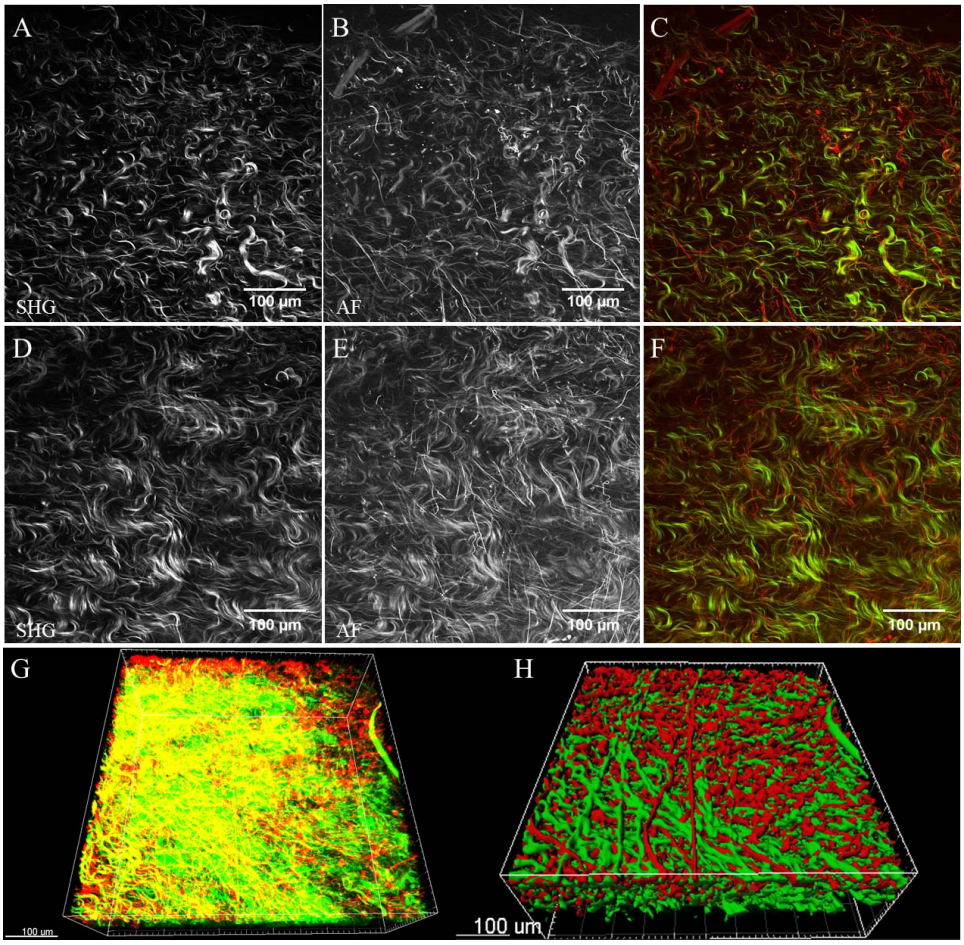

Figure 5. Two-photon excitation fluorescence microscopic images of Tenon's capsule. (**A**, **D**) Second harmonic generation image shows sinusoidal collagen bundles with high signal. (**B**, **E**) Autofluorescence image shows linear and elongated elastin fibers with high signal intensity scattered among collagen bundles with medium signal intensity. (**C**, **F**) Merged images of (**A**) shown in *green*, (**B**) in *red*, (**D**) in *green*, and (**E**) in *red*. Elastin fibers (*red*) are readily visible against green collagen bundles as a background. The orientation of elastin and collagen fibers is independent of each other. (**G**, **H**) Three-dimensional reconstruction of SHG and AF images from Tenon to superficial sclera shows the independent orientation of elastin and collagen fibers. (**G**) Simple projection of images of *z*-stacks. (**H**) Simplified view of (**G**). (**A**–**C**) Imaged at 30-µm depth. (**D**–**F**) Imaged at 80-µm depth below the conjunctival epithelium. Images were taken from sample 3. (**G**, **H**) Imaged from sample 6.

Investigative Ophthalmology & Visual Science

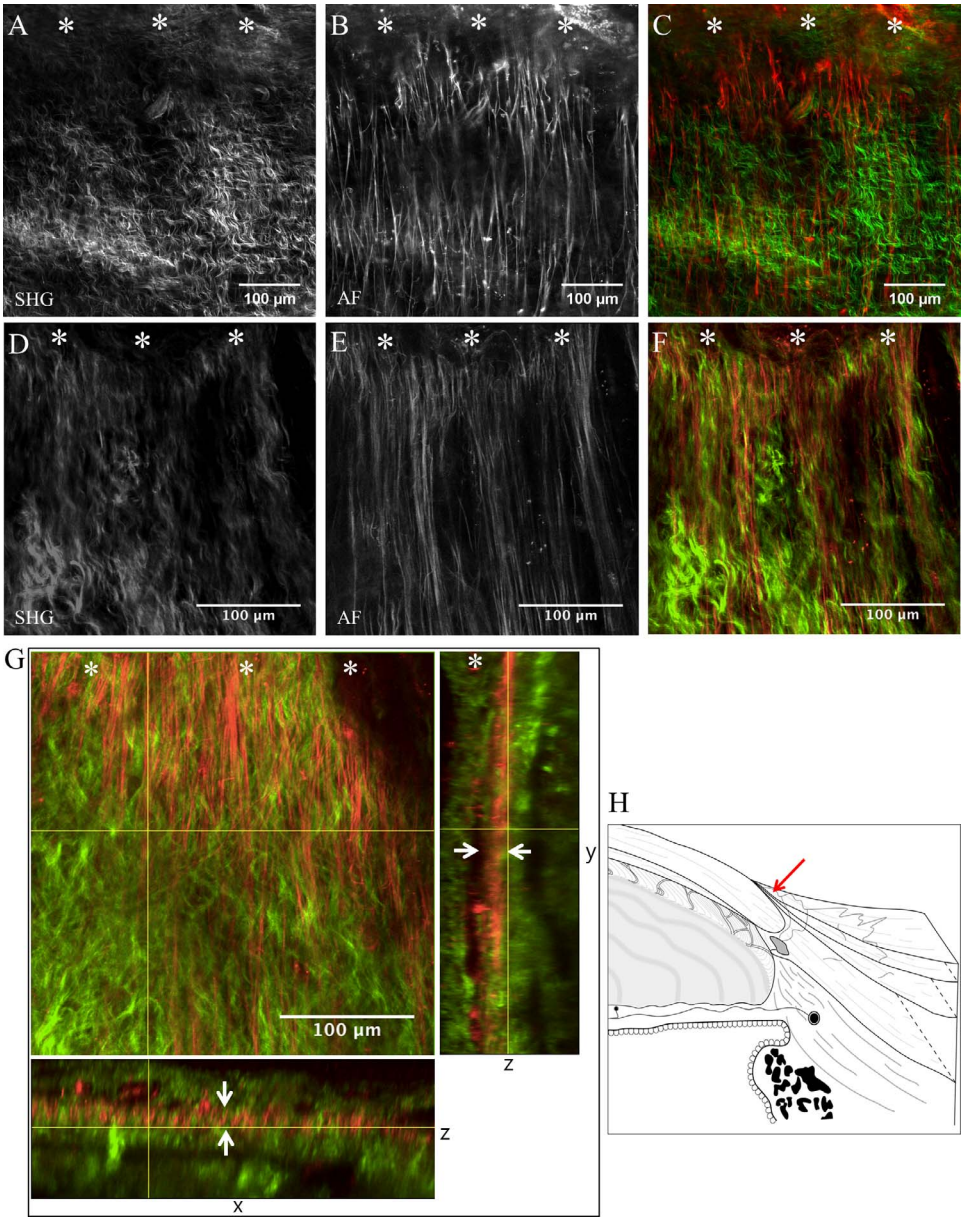

FIGURE 6. Two-photon excitation fluorescence microscopic images of Tenon's capsule near the corneal limbus. (**A**, **D**) Second harmonic generation image shows compact arrangement of wavy collagen fibers. (**B**, **E**) Autofluorescence image shows linear and elongated elastin fibers arranged perpendicular to the limbus. (**C**, **F**) Merged SHG (*green*) and AF (*red*) image panels. *Asterisks* indicate corneal limbus. (**G**) Three-dimensional reconstruction image with cross-sectional images of the crosshair-indicated planes (*y-z* plane and *x-z* plane). *Arrows* indicate bundles of elastin orthogonal to the limbus. *Asterisks* indicate limbal cornea. (**H**) Schematic image shows the area where the images were taken (*red arrow*). (**A**, **C**) Images taken from sample 4. (**D**–**G**) Images taken from sample 6.

amounts elastin fibers, which were interspersed among collagen bundles (Fig. 8).

DISCUSSION

In this study, we successfully elucidated the tangential planar collagen and elastin fiber architecture of the human conjunctiva, Tenon's capsule, and sclera by using a novel imaging technique, TPEM.

The tangential architecture of collagen and elastin in the conjunctiva, Tenon's capsule, and sclera has been poorly understood, although these structures are very important in ophthalmic clinical and surgical practice. For example, these structures are penetrated in sclera-tunnel cataract incisions. The extensive fibrosis of Tenon's capsule as the result of an abnormal increase of collagen fibers is the main cause of glaucoma filtration surgery failure and may also contribute to pterygium recurrence.[18,19] Additionally, the biomechanical strength of collagen and elastin networks determines scleral rigidity, which can affect myopic progression or development of glaucomatous optic nerve damage.[20]

It has been previously known that collagen fiber size and density increase with depth in both conjunctiva and Tenon's capsule. Our finding is also consistent with this. However, tangential serial images of nonfixed tissue by TPEM revealed novel findings in this study. We found that the diameter as well as the arrangement of collagen bundles changes at increased depths below the superficial conjunctiva. In addition, the

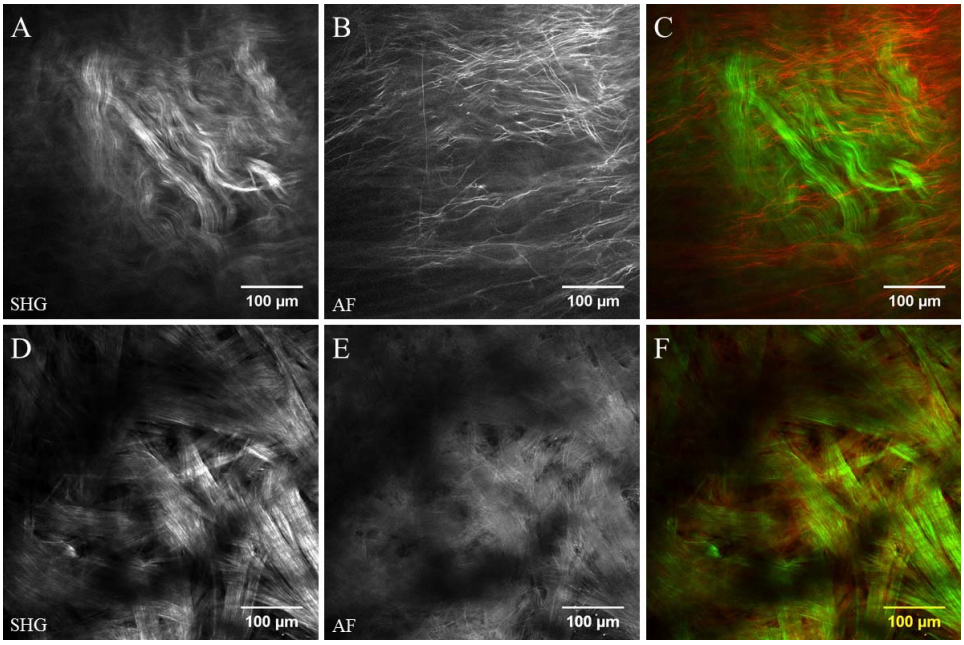

FIGURE 7. Two-photon excitation fluorescence microscopic images of superficial and deep sclera. (**A–C**) Images from superficial sclera: (**A**) SHG, (**B**) AF, (**C**) merged. (**D–F**) Images from deep sclera: (**D**) SHG, (**E**) AF, (**F**) merged. The collagen bundle arrangements of two different scleral layers differ significantly. The superficial sclera contains mostly wavy collagen bundles (**A**) with a long elastin fiber network crossing collagen bundles at almost perpendicular angles (**B**). In contrast, deep scleral collagen bundles are straighter (**D**) with an elastin fiber network interspersed among collagen bundles (**E**). Images were taken from sample 4.

orientation of both collagen and elastin fibers are independent of each other in the conjunctiva, Tenon's capsule, and superficial sclera. This suggests that collagen and elastin networks act independently to support conjunctival and Tenon's capsule integrity. This bolsters the theory that the main function of collagen fibers is to provide mechanical strength, while elastin provides elasticity, the recovery power from deformation. Moreover, despite heavy collagen fiber content, the conjunctiva and Tenon's capsule are highly elastic. A possible explanation may be the sinusoidal collagen structures found in these layers.

It is interesting that the collagen architecture was different between superficial and deeper layers of the sclera. At the superficial sclera, collagen fibers maintained a low-frequency sinusoidal appearance, although the bundle sizes were larger than those found in the Tenon's capsule. However, collagen fibers in deep sclera lost their sinusoidal appearance and were arranged in a dense linear "woven basket" network. Major differences were also noted in the elastin fiber arrangement of the superficial and deep sclera, suggesting that the biomechanics of the superficial and deep sclera are different. Another interesting finding was the distribution of abundant short elastin fibers in spaces between large collagen bundles in deep sclera. This may point toward a key role for elastin fibers in scleral elasticity. It has previously been shown that scleral elasticity increases in eyes with myopia.[9,21] Comparing collagen and elastin fiber architecture between hyperopic and myopic eyes may provide clues to understand the pathogenesis of these two refractive diseases.

In general, elastin fibers are oriented in the direction of mechanical stress.[22] Scleral elastic fibers near the optic nerve head and at the lamina cribrosa are oriented to reinforce the optic nerve head opening and resist circumferential expansion by increased intraocular pressure.[8] The typical perpendicular elastic fibers at the superficial limbus area found in this study indicate that the main mechanical stress in this area is radial. The random orientation of elastic fibers in other areas of conjunctiva and Tenon's capsule suggests no typical directionality of mechanical stress.

It is noteworthy that SHG imaging has been actively used in ophthalmic research for the past decade and has revealed the detailed collagen architecture of human cornea, sclera, and optic nerve head.[10,15,23–25] By using the SHG imaging technique, successful demonstration of compact and regular collagen fiber distribution of corneal stroma was reported and it was distinguished from irregular scleral collagen fiber distribution.[10,26] In another study, the density difference of collagen fibers at different regions of lamina cribrosa was analyzed based on SHG images and nonuniform mechanical stress of this structure was suggested as the possible mechanism of axonal damage.[25] In our study, we combined AF and SHG images to evaluate collagen architecture in conjunction with elastin architecture. The pattern variation as a function of depth in the ocular coat may suggest that mechanical stress also varies as a function of tissue depth.

To our knowledge, this is one of the first reports detailing elastin and collagen architecture of the conjunctiva and Tenon's capsule in nonfixed human tissue. Although clinical confocal microscopy may provide high resolution imaging of the conjunctiva and cornea at the cellular level,[5,27] the existing technology cannot distinguish collagen and elastin fibers as one can with TPEM.[17] Thus several clinical applications of TPEM are anticipated. For example, collagen and elastin fiber characteristics of filtering blebs may possibly be useful to estimate filtering function and may be a predictor for encapsulation and subsequent failure.[28] Collagen and elastin fiber architecture and density at pterygium resection margins may also be used to monitor signs of early recurrence.[29] Finally, the potential to diagnose invasive corneal or conjunctival epithelial neoplasms that can destroy underlying collagen architecture may be another valuable clinical application of TPEM technology.[30,31]

This study had several limitations. The images were taken from donor corneoscleral buttons. The attached conjunctiva,

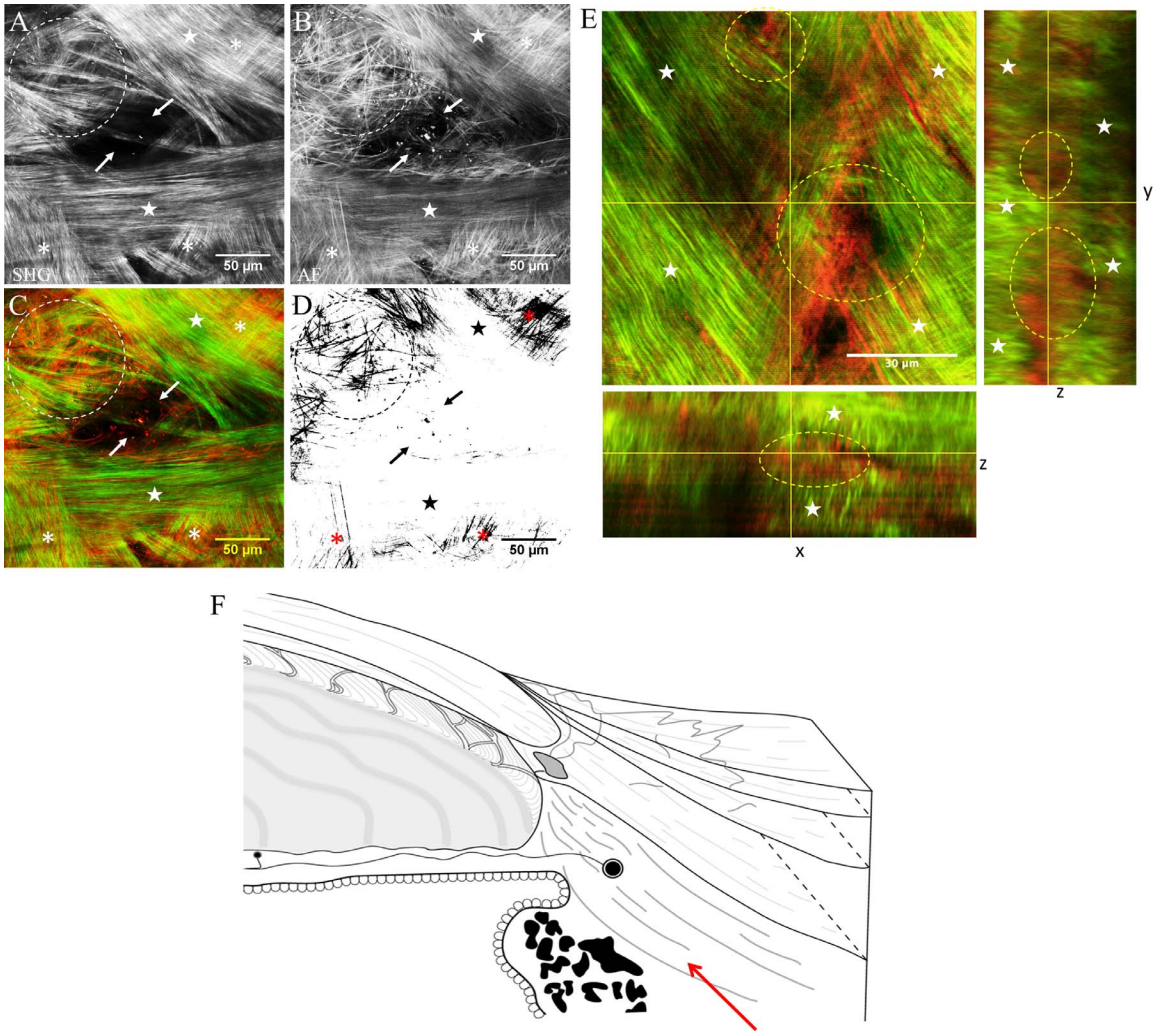

Figure 8. Two-photon excitation fluorescence microscopic images of deep sclera. (**A**) Second harmonic generation image shows a typical "woven basket" appearance of collagen bundles in deep sclera. *Arrows* indicate spaces for penetrating vessels. (**B**) Autofluorescence imaging shows a fine and short elastin network connecting two collagen bundle structures (*dotted circle*). Another heavy elastin network is visible where two collagen bundles cross (*asterisks*). (**C**) Merged image of (**A**) shown in *green*, and (**B**) in *red*. *Stars* in (**A**–**C**) indicate the same two large collagen bundles. (**D**) *Black and white* binary image (ImageJ → Subtract image A from image B → Make binary); deleted collagen signals and shows the elastin network only. (**E**) Volume analysis of deep sclera revealed the elastin network (*yellow dotted circle*) is located between thick scleral collagen fibers (*stars*). (**F**) Schematic image shows the area where the images were taken (*red arrow*). (**A**–**D**) Images were taken from sample 5. (**E**) Image was taken from sample 7.

Tenon's capsule, and sclera were limited to several millimeters in length around the cornea. Therefore, the images of distal tissue near extraocular muscles or beyond were impossible. Furthermore, the native mechanical tension of these tissues was significantly altered with trephination at the donor tissue margin. It is possible that the wavy collagen architecture observed at the conjunctiva and Tenon's capsule were related to the loss of distal anchoring and attachment only at the proximal end. Unfortunately, there is currently no available TPEM system to image live human ocular structures. In addition, it should be noted that characterization of collagen fibers obtained with SHG imaging can be significantly affected by the degree of tissue edema and scattering directions.[26,32] The forward scattered signal of SHG can show different collagen characteristics compared with the backward signal.[26,32] As another limitation, small sample size limited us to perform comparative studies about SHG and AF signals according to imaging locations in the same donor and donor characteristics such as age, sex, and race. This comparative study can be an interesting topic for future investigation.

In summary, we have elucidated the collagen and elastin architecture of the human conjunctiva, Tenon's capsule, and superficial sclera by using TPEM. The characteristic patterns of these fibers were successfully demonstrated in serial tangential image planes. When considering the noninvasive nature of TPEM, the potential for future clinical applications in ophthalmology is promising.

Acknowledgments

The authors thank the Central Florida Lions Eye and Tissue Bank (Tampa, FL, USA) and Saving Sight Eye Bank (Kansas City, MO, USA) for their tissue support, and the Analytical Imaging Facility of Albert Einstein College of Medicine for technical support.

Supported by a grant from the Korea Health Technology R&D Project through the Korea Health Industry Development Institute (KHIDI), Ministry of Health & Welfare, Republic of Korea (Grant No. HI-15C1653); a core grant from Research to Prevent Blindness

(Albert Einstein College of Medicine); and Cancer Center Support Grant No. P30 CA013330. The authors alone are responsible for the content and writing of the paper.

Disclosure: **C.Y. Park**, None; **C.M. Marando**, None; **J.A. Liao**, None; **J.K. Lee**, None; **J. Kwon**, None; **R.S. Chuck**, None

References

1. Leong YY, Tong L. Barrier function in the ocular surface: from conventional paradigms to new opportunities. *Ocul Surf*. 2015;13:103–109.
2. Braun RJ, King-Smith PE, Begley CG, Li L, Gewecke NR. Dynamics and function of the tear film in relation to the blink cycle. *Prog Retin Eye Res*. 2015;45:132–164.
3. Schultz DS, Lotz JC, Lee SM, Trinidad ML, Stewart JM. Structural factors that mediate scleral stiffness. *Invest Ophthalmol Vis Sci*. 2008;49:4232–4236.
4. Marshall GE. Human scleral elastic system: an immunoelectron microscopic study. *Br J Ophthalmol*. 1995;79:57–64.
5. Meek KM, Fullwood NJ. Corneal and scleral collagens–a microscopist's perspective. *Micron*. 2001;32:261–272.
6. Austin P, Jakobiec FA, Iwamoto T. Elastodysplasia and elastodystrophy as the pathologic bases of ocular pterygia and pinguecula. *Ophthalmology*. 1983;90:96–109.
7. Ostrin LA, Wildsoet CF. Optic nerve head and intraocular pressure in the guinea pig eye. *Exp Eye Res*. 2015;146:7–16.
8. Gelman S, Cone FE, Pease ME, Nguyen TD, Myers K, Quigley HA. The presence and distribution of elastin in the posterior and retrobulbar regions of the mouse eye. *Exp Eye Res*. 2010; 90:210–215.
9. McBrien NA, Jobling AI, Gentle A. Biomechanics of the sclera in myopia: extracellular and cellular factors. *Optom Vis Sci*. 2009;86:E23–E30.
10. Morishige N, Petroll WM, Nishida T, Kenney MC, Jester JV. Noninvasive corneal stromal collagen imaging using two-photon-generated second-harmonic signals. *J Cataract Refract Surg*. 2006;32:1784–1791.
11. Ammar DA, Lei TC, Gibson EA, Kahook MY. Two-photon imaging of the trabecular meshwork. *Mol Vis*. 2010;16:935–944.
12. Zipfel WR, Williams RM, Webb WW. Nonlinear magic: multiphoton microscopy in the biosciences. *Nat Biotechnol*. 2003;21:1369–1377.
13. Chu ER, Gonzalez JM Jr, Tan JC. Tissue-based imaging model of human trabecular meshwork. *J Ocul Pharmacol Ther*. 2014; 30:191–201.
14. Winkler M, Chai D, Kriling S, et al. Nonlinear optical macroscopic assessment of 3-D corneal collagen organization and axial biomechanics. *Invest Ophthalmol Vis Sci*. 2011;52: 8818–8827.
15. Park CY, Lee JK, Chuck RS. Second harmonic generation imaging analysis of collagen arrangement in human cornea. *Invest Ophthalmol Vis Sci*. 2015;56:5622–5629.
16. Park CY, Lee JK, Kahook MY, Schultz JS, Zhang C, Chuck RS. Revisiting ciliary muscle tendons and their connections with the trabecular meshwork by two photon excitation microscopic imaging. *Invest Ophthalmol Vis Sci*. 2016;57:1096–1105.
17. Park CY, Lee JK, Zhang C, Chuck RS. New details of the human corneal limbus revealed with second harmonic generation imaging. *Invest Ophthalmol Vis Sci*. 2015;56:6058–6066.
18. Choritz L, Grub J, Wegner M, Pfeiffer N, Thieme H. Paclitaxel inhibits growth, migration and collagen production of human Tenon's fibroblasts–potential use in drug-eluting glaucoma drainage devices. *Graefes Arch Clin Exp Ophthalmol*. 2010; 248:197–206.
19. Touhami A, Di Pascuale MA, Kawatika T, et al. Characterisation of myofibroblasts in fibrovascular tissues of primary and recurrent pterygia. *Br J Ophthalmol*. 2005;89:269–274.
20. Sergienko NM, Shargorogska I. The scleral rigidity of eyes with different refractions. *Graefes Arch Clin Exp Ophthalmol*. 2012;250:1009–1012.
21. Pekel G, Agladioglu K, Acer S, Bozkurt K, Cetin EN, Yagci R. Evaluation of ocular elasticity in high myopia. *Optom Vis Sci*. 2015;92:573–578.
22. Chow MJ, Turcotte R, Lin CP, Zhang Y. Arterial extracellular matrix: a mechanobiological study of the contributions and interactions of elastin and collagen. *Biophys J*. 2014;106: 2684–2692.
23. Jester JV, Winkler M, Jester BE, Nien C, Chai D, Brown DJ. Evaluating corneal collagen organization using high-resolution nonlinear optical macroscopy. *Eye Contact Lens*. 2010;36: 260–264.
24. Brown DJ, Morishige N, Neekhra A, Minckler DS, Jester JV. Application of second harmonic imaging microscopy to assess structural changes in optic nerve head structure ex vivo. *J Biomed Opt*. 2007;12:024029.
25. Winkler M, Jester B, Nien-Shy C, et al. High resolution three-dimensional reconstruction of the collagenous matrix of the human optic nerve head. *Brain Res Bull*. 2010;81:339–348.
26. Han M, Giese G, Bille J. Second harmonic generation imaging of collagen fibrils in cornea and sclera. *Opt Express*. 2005;13: 5791–5797.
27. Kymionis GD, Diakonis VF, Shehadeh MM, Pallikaris AI, Pallikaris IG. Anterior segment applications of in vivo confocal microscopy. *Semin Ophthalmol*. 2015;30:243–251.
28. Van de Velde S, Van Bergen T, Vandewalle E, Moons L, Stalmans I. Modulation of wound healing in glaucoma surgery. *Prog Brain Res*. 2015;221:319–340.
29. Sun CK, Yu CH, Tai SP, et al. In vivo and ex vivo imaging of intra-tissue elastic fibers using third-harmonic-generation microscopy. *Opt Express*. 2007;15:11167–11177.
30. Teh SK, Zheng W, Li S, et al. Multimodal nonlinear optical microscopy improves the accuracy of early diagnosis of squamous intraepithelial neoplasia. *J Biomed Opt*. 2013;18: 036001.
31. Thomas G, van Voskuilen J, Truong H, Gerritsen HC, Sterenborg HJ. In vivo nonlinear optical imaging to monitor early microscopic changes in a murine cutaneous squamous cell carcinoma model. *J Biophotonics*. 2015;8:668–680.
32. Hsueh CM, Lo W, Chen WL, et al. Structural characterization of edematous corneas by forward and backward second harmonic generation imaging. *Biophys J*. 2009;97:1198–1205.

Investigative Ophthalmology & Visual Science